A Hückel model for the excited state dynamics of a protein chromophore developed using photoelectron imaging

Cate S. Anstöter and Jan R. R. Verlet†*

Department of Chemistry, Durham University, Durham DH1 3LE, United Kingdom

*csanstoter@gmail.com

†j.r.r.verlet@durham.ac.uk

Conspectus

Chemistry can be described as the movement of nuclei within molecules and the concomitant instantaneous change in electronic structure. This idea underpins the central chemical concepts of potential energy surfaces and reaction coordinates. To experimentally capture such chemical change therefore requires methods that can probe both the nuclear *and* electronic structure simultaneously and on the timescale of atomic motion. In this Account, we show how time-resolved photoelectron imaging can do exactly this and how it can be used to build a detailed and intuitive understanding of the electronic structure and excited state dynamics of chromophores. The chromophore of the photoactive yellow protein (PYP) is used as a case study. This chromophore contains a *para*-substituted phenolate anion, where

the substituent, R, can be viewed as an acrolein derivative. It is shown that the measured photoelectron angular distribution can be directly related to electronic structure of the *para*-substituted phenolate anion. By incrementally considering differing R groups, it is also shown that these photoelectron angular distributions are exquisitely sensitive to the conformational flexibility of R and that, when R contains a π-system, the excited states of the chromophore can be viewed as a linear combination of the π* molecular orbitals on the phenolate (π_{Ph}*) and R-substituent (π_R*). Such a Hückel treatment shows that the S_1 state of the PYP chromophore is predominantly of π_R* character and that it is essentially the same as the chromophore of the green fluorescent protein (GFP). The S_1 excited state dynamics of the PYP chromophore probed by time-resolved photoelectron imaging clearly reveal both structural (nuclear) dynamics through the energy spectrum, as well as electronic dynamics through the photoelectron angular distributions. Both motions can be accurately assigned using quantum chemical calculations and these are consistent with the intuitive Hückel treatment presented. The photoactive protein chromophores considered here are examples of where a chemists' intuitive Hückel view for ground state chemistry appears to be transferable to predict photochemical excited state reactivity. While elegant and insightful, such models have limitations, including non-adiabatic dynamics, which is present in a related PYP chromophore, where a fraction of the S_1 state population forms a non-valence (dipole-bound) state of the anion.

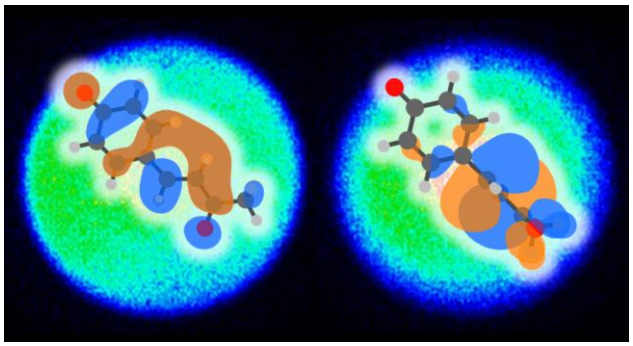

Key References

- Anstöter, C. S.; Curchod, B. F. E.; Verlet, J. R. R. Geometric and electronic structure probed along the isomerisation coordinate of a photoactive yellow protein chromophore *Nat. Comm.* **2020**, *11*, 282. [1] *The electronic and nuclear dynamics are resolved along the isomerization coordinate of the PYP chromophore using time-resolved photoelectron imaging and electronic structure calculations.*

- Anstöter, C. S.; Dean, C. R.; Verlet, J. R. R. Chromophores of chromophores: A bottom-up Hückel picture of the excited states of photoactive proteins *Phys. Chem. Chem. Phys.* **2017**, *19*, 29772. [2] *A Hückel picture to explain the excited states of the PYP and GFP chromophores is presented based on a linear combination of the lowest unoccupied molecular orbitals on phenolate and the para-substituted fragment.*

- Anstöter, C. S.; Dean, C. R.; Verlet, J. R. R. Sensitivity of Photoelectron Angular Distributions to Molecular Conformations of Anions *J. Phys. Chem. Lett.* **2017**, *8*, 2268. [3] *This study shows how the photoelectron emission angle for a para-substituted phenolate anion depends sensitively on the conformation of the substituent.*

- Bull, J. N.; Anstöter, C. S.; Verlet, J. R. R. Ultrafast valence to non-valence excited state dynamics in a common anionic chromophore *Nat. Comm.* **2019**, *10*, 5820. [4] *The isomerization dynamics in a PYP chromophore are shown to compete with internal conversion to a non-valence dipole-bound state of the anion, which can be clearly identified through time-resolved photoelectron imaging.*

Introduction

Light-driven processes are common in biology and are central to phototaxis, vision, and photosynthesis. While the biological response involves large proteins and protein complexes, the initial photo-induced process typically involves a small molecular chromophore that acts as a light-sensitive transducer to mechanically initiate a large-scale response.[5] This transduction often takes the form of isomerisation about specific bonds.[6] Understanding the initial motion and how light activates biological function has been widely studied for many years and was amongst the first processes to be studied in real-time.[7] An ultimate goal is to completely understand the excited state dynamics taking place in the chromophore and its immediate surrounding, so that the chromophore may be adapted and controlled to drive a specific outcome, be it more efficient transduction to mechanical motion (e.g. for in vision) or enhanced fluorescence (e.g. for in signalling or communication). To gain such insight, studying the chromophore in isolation from the protein environment has been very useful.[8] Using this bottom-up approach offers a window into the intrinsic photo-physics of the chromophore and is amenable to high-level calculations, the combination of which can yield the foundational understanding of the initial chemical dynamics. Over the years, virtually all studies with these goals in mind have focussed on how the nuclei move following photoexcitation. However, ignoring the *electronic* evolution essentially ignores the basic premise of chemistry – that the electronic character adiabatically evolves with nuclear motion (the Born-Oppenheimer approximation). To fully understand chemical dynamics, both the electronic *and* nuclear dynamics should be probed in unison. There have been exquisite experiments in recent years to achieve this goal, but most have focussed on very small molecular species through complex experimental methods that are not easily extended to the size of the chromophores involved in photo-biology.[9–13] We have recently developed methods to bridge this by using time-resolved photoelectron imaging of anions in conjunction

with computational methods. In this Account, we describe how such experiments provide the required information, and how this has offered an understanding of the structure of bio-chromophores based on substituted phenolate anions.

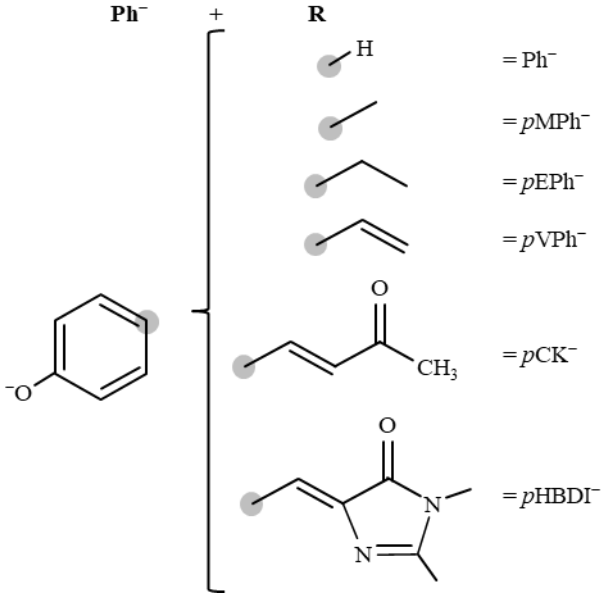

Figure 1: Structures of *para*-substituted (with groups R) phenolate anions considered: Ph^- = phenolate, *p*MPh^- = *p*-methylphenolate; *p*EPh^- = *p*-ethylphenolate; *p*VPh^- = *p*-vinylphenolate; *p*CK^- = *p*-coumaric ketone; and *p*$HBDI^-$ = *p*-hydroxybenzylidene-1,2-dimethylimidazoline.

The phenolate anion is a common motif in nature and photoactive proteins, with well-known examples including the green fluorescent protein (GFP) and the photoactive yellow protein (PYP). Here, we will focus on the latter. PYP is a protein that acts to induce negative phototaxis in response to blue light in several bacterial organisms.[14] The chromophore of PYP is a para-coumaric acid that is commonly modelled by a *p*-coumaric ketone (*p*CK^-, Figure 1).[15] PYP and its chromophore have often been used to demonstrate new experimental methods to probe its nuclear dynamics, with examples including: time-resolved photoelectron spectroscopy,[16] fifth-order time-domain Raman spectroscopy,[17] and serial time-resolved X-ray diffraction at free-electron lasers.[18] Here, we develop the former of these further and show how additional differential measurements on the photoelectrons offer concomitant

insight into the *electronic* evolution. In addition, we unpick the electronic structure by through use of a simple model based on Hückel theory in which the chromophore is built up of molecular sub-units. This model offers useful and intuitive chemical insight, especially with a view to designing and modifying the photophysical properties of chromophores.

Photoelectron imaging of anions formed by electrospray ionisation

Photoelectron spectroscopy of gas-phase species determines the binding energy of electrons in molecules. Within a Koopmans' picture, it effectively measures the orbital energy difference between a molecule with N and one with $N - 1$ electrons. With the advent of charged-particle imaging and specifically velocity-map imaging,[19] the already differential method of photoelectron spectroscopy gained a further dimension as both the magnitude and direction of photoelectron velocity vectors could be measured. The photoelectron angular distribution (PAD) is sensitive to the molecular orbital from which the electron is detached. In the molecular frame, this correlation is very well-defined. However, even in a laboratory-frame, despite the averaging that takes place over the initial orientational distributions, the PADs retain information about the electronic structure[20] and this information will be discussed here for chromophores based on para-substituted phenolate anions. The PADs are generally quantified using an anisotropy parameter, β_2, which can vary from –1 to +2 for a single-photon transition: when $\beta_2 = +2$, electrons are emitted predominantly parallel to the polarisation axis of the light, $\boldsymbol{\varepsilon}$; when $\beta_2 = -1$, electrons are emitted predominantly perpendicular to $\boldsymbol{\varepsilon}$; and when $\beta_2 = 0$, emission is isotropic.[20,21]

There are some key benefits to probing anions (rather than more commonly studied neutral molecules). Firstly, because the electron affinity of a molecule is generally much lower than its ionisation energy, detaching of an electron from an anion requires lower photon energies (typically in a range < 5 eV).[22,23] Secondly, the fact that the anion is charged

allows for mass-selection *prior* to its photoelectron spectroscopy so that the sample is pure (although isomers/conformers and isobaric species could be present). Thirdly, ion sources such as electrospray ionisation or matrix assisted laser desorption can be used to generate the anions, which open-up a vast range of molecular systems that would otherwise not be possible to study using commonly used molecular beam methods for neutral molecules. Details of our home-built instrument that incorporates electrospray ionisation with time-of-flight mass spectrometer and velocity map imaging has been described in detail elsewhere.[24,25]

Photoelectron angular distributions as a window into geometric and electronic structure

The PYP chromophore is a para-substituted phenolate, Figure 1, and we therefore start by considering the effect of substitution on the photoelectron spectra and PADs. The photoelectron images and spectra of the phenolate anion with a para-substituted methyl (*p*MPh$^-$), ethyl (*p*EPh$^-$), and vinyl (*p*VPh$^-$) group are shown in Figure 2.[2] The photoelectron images, Figure 2(a), were taken at $h\nu$ = 2.85 eV and $\boldsymbol{\varepsilon}$ is indicated. The only available channel for detachment at this energy is to the ground state of the neutral molecule. In all three cases, the photoelectron images have a similar radial extent. Indeed, when extracting the photoelectron spectra from these images, Figure 2(b), the overall spectral shape and binding energies of the photoelectron spectrum from the three molecular anions is very similar. However, the PADs associated with this seemingly similar detachment channel are very different across the three systems. For detachment from *p*MPh$^-$ and *p*VPh$^-$, the overall emission is perpendicular to the polarisation axis; β_2 is negative. In contrast, the emission for *p*EPh$^-$ appears significantly more isotropic implying that $\beta_2 \sim 0$. In Figure 2(c), β_2 is extracted from photoelectron images over a series of $h\nu$ to allow the evolution of β_2 as a function of the electron kinetic energy (eKE) to be extracted. Note that the eKE axes in Figure 2(b) and (c)

are therefore not the same, with the latter corresponding to several measurements rather than the single measurement in the former. These plots clearly confirm the observation of differing behaviours (even qualitative) of β_2 for *p*EPh$^-$ compared to *p*MPh$^-$ and *p*VPh$^-$. Data is only considered over the first 1 eV of the continuum; beyond this, metastable excited states of the anion (resonances) are accessed, leading to dramatic changes in the PADs.

Also shown in Figure 2(c) are results of computed PADs, predicted using the Dyson orbital approach[26] within the equation-of-motion ionisation-potential coupled cluster singles and doubles formalism (EOM-IP-CCSD). The Dyson orbital, Ψ_D, can be thought of as the one-electron orbital from which the electron is removed upon photodetachment. With knowledge of Ψ_D, the PADs can be calculated using, for example, the eZDyson package developed by Krylov and coworkers.[27] Details of the method and a benchmarking study exploring its application to anions[28] has been described previously and are will not be considered further here. Importantly, in the cases considered here, the PADs are always laboratory-frame observables. Note also that simple symmetry arguments can be formulated to account for the overall sign of β_2, which can offer added insight without the need for high-level calculations.[29]

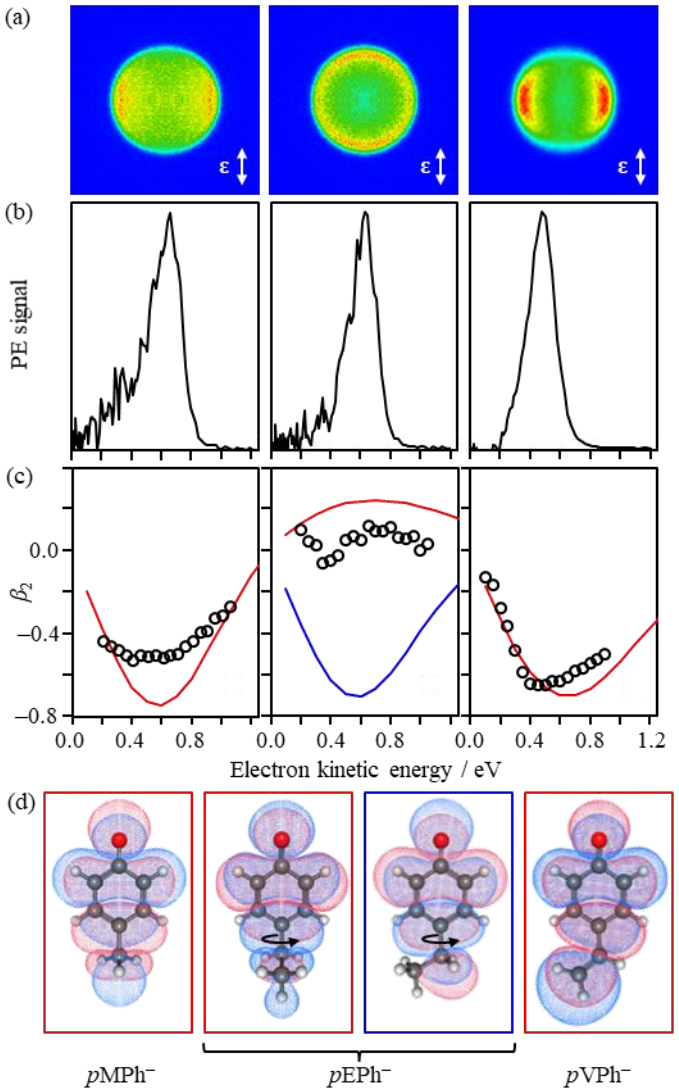

Figure 2: photoelectron spectroscopy of *p*-substituted phenolates. (a) Photoelectron images of *p*-methylphenolate, *p*-ethylphenolate, and *p*-vinylphenolate taken at $h\nu$ = 2.85 eV with polarisation axis shown by double arrows. (b) Corresponding photoelectron spectra. (c) β_2 parameters from individual measurements (circles) at differing $h\nu$ and predicted (lines) by using the Dyson orbitals shown in (d). Adapted with permission from ref. 3. Copyright 2017 American Chemical Society.

Figure 2(c) shows that the overall predicted trends for *p*MPh$^-$ and *p*VPh$^-$ are similar and in good overall agreement with the experimentally measured PADs. For *p*EPh$^-$, the situation is more complex because this substituent has as torsional degree of freedom. Specifically, the ethyl group can be in the plane of the phenolate ring or perpendicular to this plane, the latter being the lowest-energy conformation. The most striking observation here,

however, is the sensitivity of the PADs to this conformational freedom.[3] From Figure 2, the predicted β_2 trend for the in-plane conformer of *p*EPh$^-$ is similar to that of *p*MPh$^-$ and *p*VPh$^-$, while for the out-of-plane conformer, β_2 is predicted to be slightly positive. The latter is in reasonable agreement with experiment and in accord with this conformer being the most prevalent in the anion distribution.[3] The conformational differences are not apparent from the photoelectron spectra, but very clearly so from the PADs. Hence, the PADs are exquisitely sensitive to the small changes in *electronic* structure for these two conformers, with Ψ_D for all the relevant species shown in Figure 2(d). In contrast, the photoelectron spectra are dictated by the Franck-Condon factors between anion and neutral that are not sensitive to these conformation changes.

A natural extension of this work is now to track electronic evolution along a reaction coordinate in real-time, which is described below.[1] However, we first take a detour to consider the overall electronic structure of the PYP chromophore in the context of a simple Hückel theory picture.

A Hückel theory model for bio-chromophores

In general, bio-chromophores have extended polyenes (e.g. retinoids), aromatic rings (e.g. porphyrins), or both (e.g. GFP, PYP) as their chromophoric cores. In cases where both are present, one can view the electronic structure of the chromophore as a superposition of the molecular orbitals (MOs) associated with the ring and polyene. Such a view is complementary to high-level calculations, but with the benefit of its simplicity in terms of predicting how electronic structure might change through minor chemical changes, and therefore also its applicability by the broader chemical community.

An outstanding example of the success of simple Hückel approaches was demonstrated by Bravaya *et al.*,[30] in which the electronic structure of the S_1 state of different coloured

photoactive proteins was rationalised through use of a 3-centre allyl radical in a simple Hückel framework and a particle in a box model. Utilising a similar approach, Bochenkova *et al.* interpreted the electronic structure of the S_3 state of the chromophore anion of GFP (*p*-hydroxybenzylidene-2,3-dimethylimidazolinone, *p*HBDI$^-$) and its electronic excitation.[31]

Taking inspiration, we applied a modified Hückel model to develop an understanding of the electronic structure of para-substituted phenolate anions. Comparison of the photoelectron spectra of the bare phenolate anion with *p*EPh$^-$ and *p*VPh$^-$, discussed in the previous section, and *p*CK$^-$ (PYP) and *p*HBDI$^-$ (GFP), provides us with a bottom-up insight into the changing excited state as a function of substitution.[2] The 2D photoelectron spectra for Ph$^-$, *p*VPh$^-$ and *p*HBDI$^-$ are shown in Figure 3(a-c). All three are broadly similar: spectra are dominated by a feature for which the eKE increases linearly with increasing *hv*. This corresponds to the direct detachment channel discussed previously. The onset of a second direct detachment channel (in which the neutral is left in the first excited D_1 state), is seen clearly for Ph$^-$ starting at *hv* ~ 3.2 eV. In addition to the direct detachment features, spectral broadening is seen for all anions over a *hv* range, in which the signal from the high eKE channel shifts to lower eKE (e.g. at *hv* ~ 3.7 eV in Figure 3(a)) .[2] Concurrent with the spectral broadening, abrupt changes were also observed in the PADs, indicative of a change in the molecular orbital (MO) from which the electron is lost. Both the broadened spectral signature and the abrupt changes to the PADs thus point to the presence of excited states of the anion, from which the electron is lost via autodetachment (*i.e.* resonances).[32–34] The locations of these excited states are indicated in Figure 3.

Our interest is in understanding the electronic structure of the excited states. Consider the phenolate moiety. The lowest unoccupied MO corresponds to a π* orbital, π_{Ph}*, and the π_{Ph}* ← π_{Ph} is the lowest energy transition (*i.e.* $S_1 \leftarrow S_0$), seen in Figure 3(a). Because π_{Ph}* has a node along the O and the carbon in the *para*-position, the addition of an alkyl-group here

does not affect π_{Ph}* (σ-π separability) and the 2D photoelectron spectra and PADs of Ph^-, *p*MPh^- and *p*EPh^- are all very similar. In the case of *p*VPh^- and *p*$HBDI^-$, the R-group has its own π-system, with a corresponding empty antibonding MO, π_R*. The electronic structure is now defined as a linear combination of π_{Ph}* and π_R*.

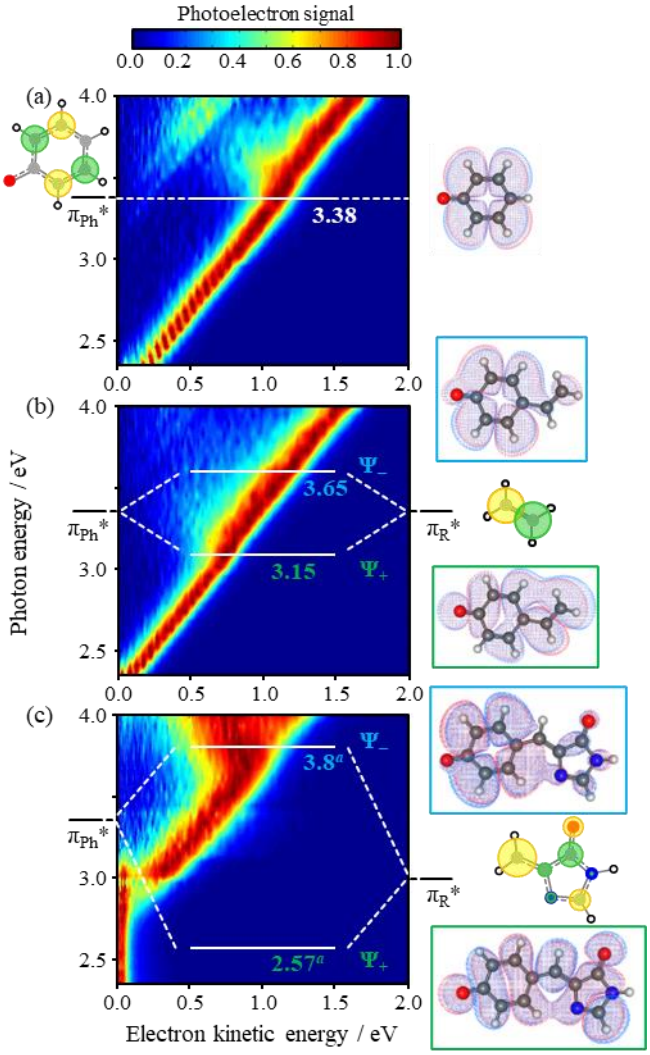

Figure 3: 2D photoelectron spectra of (a) phenolate, (b) *p*-vinylphenolate, and (c) *p*HDBI. Included is the energy of the resonances associated with the phenolate LUMO (π_{Ph}*) and the LUMO energy of the *para*-substituent R (π_R*) along with the Hückel MOs. These combine as a linear combination of MOs to form the MOs Ψ_+ and Ψ_- that are associated with the S_1 and S_2 excited states of the *p*-vinylphenolate and S_1 and S_3 of *p*HDBI. Adapted with permission from ref. 2. Copyright 2017 Royal Society of Chemistry.

For *p*VPh$^-$, two resonances are observed, Figure 3(b). First, consider the Hückel energy of π_{Ph}*. Given a node encompasses the O atom, the orbital energy of π_{Ph}* is that of the π* MO of benzene, $\varepsilon = \alpha - \beta$. When considering R, the C atom of the phenyl ring should be excluded. Thus, for *p*VPh$^-$, R is ethene and π_R* is the π* MO of ethene which also has a Hückel energy $\varepsilon = \alpha - \beta$. Hence, the π_{Ph}* and π_R* MOs are degenerate in this simple picture and a linear combination of the π_{Ph}* and π_R* yields the two overall MOs: $\Psi_\pm = 2^{-½}\pi_{Ph}^* \pm 2^{-½}\pi_R^*$. This is in excellent agreement with the observations for *p*VPh$^-$, which show that the two resonances are split by ~0.2 eV either side of the π_{Ph}* resonance (i.e. $\beta \sim -0.2$ eV) (Figure 3(b)). It is also in agreement with electronic structure calculations,[2] with the molecular orbitals associated with Ψ_+ and Ψ_- shown in Figure 3(b).

The same Hückel framework can now be scaled to any R group to offer a rather intuitive insight into the excited states of the chromophores. We first consider the GFP chromophore, *p*HBDI$^-$, in Figure 3(c).[35] In our model, R is 2-ethene-imidazole (methyl groups can be neglected as they have little effect on the π-electronic structure). The Hückel energy of π_R* is $\varepsilon = \alpha - 0.35\beta$. The resultant Ψ_+ and Ψ_- MOs have a larger separation and their character will be dictated by the coefficients in the linear combination. For Ψ_+ (associated with S_1) the π_R* coefficients will be much larger than those for π_{Ph}*. Hence, the S_1 state will have predominantly π_R* character. The higher lying excited state associated with Ψ_- will have predominantly π_{Ph}* character. These qualitative predictions are broadly consistent with both experiment and high-level electronic structure calculations. In *p*HBDI$^-$, the S_1 state is bound (*i.e.* lies below the D_0 level[36,37]) and indeed has predominantly π_R* character according to high-level extended multi-configurational quasi-degenerate perturbation theory (XMQCDPT2) calculations.[38] The excited state associated with Ψ_- can also be seen in experiment (Figure 3(c)) and using computational chemistry, but it is the S_3 state as there is an additional S_2 core-excited state that a simple Hückel model cannot account for.[31] Here we

focus on S_1 but note that the higher-lying states are interesting in their own right from a photo-oxidation perspective in bio-molecules.

A remarkable conclusion from the Hückel picture is that the chromophores of GFP and PYP are essentially identical! For *p*CK$^-$, R is acrolein (methyl vinyl ketone with the methyl group ignored) and in Figure 4, the π_R* MOs of *p*HBDI$^-$ and *p*CK$^-$ are shown, demonstrating their striking similarity. The similarity comes about because of the very small coefficients on the N atoms in 2-ethene-imidazole and this conclusion is in agreement with both the high-level calculations and experiment. The S_1 state in *p*CK$^-$ is similarly bound and the S_3 state can be identified with predominant π_{Ph}* character.

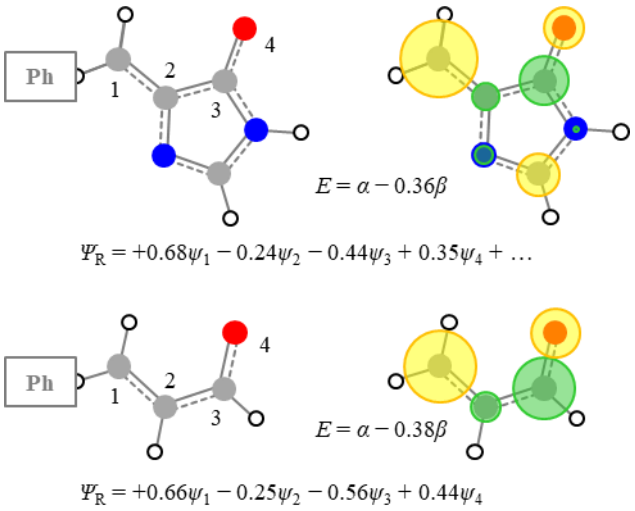

Figure 4: Structure and lowest unoccupied Hückel MOs of the *para*-substituents 2-ethene-imidazole and acrolein to represent the chromophores of GFP and PYP, respectively. Also shown is the orbital energy and the wavefunction of these MOs, showing the similarity between the two.

Using the above insight and the conclusion that the S_1 state of *p*CK$^-$ has predominantly π_R* character, we now return to considering how the electronic changes can be tracked along a reaction coordinate using *p*CK$^-$ as an example.[1]

Nuclear and electronic structure simultaneously measured along an isomerisation coordinate

While single photon photoelectron imaging can probe the ground state anion as described above, an excited state can be probed in a two-colour pump-probe scheme. For *p*CK$^-$, the S_1 state dynamics were probed by initially exciting with a short pump pulse at 2.79 eV (444 nm) and subsequently probed at 1.55 eV (800 nm) by a second delayed short probe pulse. The excitation energy was finely tuned to excite the S_1 state while minimizing direct detachment. The photoelectron image generated by the probe is a measure of the S_1 state at the time it was probed, and its evolution can this be tracked through the $S_1 + h\nu_{probe} \rightarrow D_0 + e^-$ detachment channel.[1]

Excitation to the S_1 state leads to a weakening of the π system which enables isomerization. This isomerization can proceed along either the "single-bond" connecting the phenyl ring to the para-substituted methyl vinyl ketone, φ_{SB}, or along the "double-bond" in the fragment, φ_{DB}, as shown in Figure 5(a).[39]

Figure 5(b) shows the results of the experiment, where photoelectron spectra are presented as difference spectra in which any small signal at $t < 0$ has been subtracted from all time-resolved images to leave only the excited state signals.[1] At eKE < 0.05 eV, this leads to a negative signal, which arises from the bleaching of the small contribution of direct detachment and/or autodetachment. The main features of interest are associated with the positive photoelectron signal at eKE > 0.2 eV, as these represent the evolution of the S_1 state. At $t = 0$, the photoelectron signal peaks at eKE ~ 1.3 eV. This then appears to decay and form a new feature peaking at eKE ~ 0.8 eV, but additionally shows a coherence in which populations oscillates once between these two features, before settling. At times beyond 1 ps, the high eKE feature decays leaving only the peak at eKE ~ 0.8 eV and this subsequently

decays with a timescale of ~120 ps.[1] Here we focus on the first ps of the dynamics and two representative photoelectron spectra at t = 0 and t = 1 ps are shown in Figure 5(c).

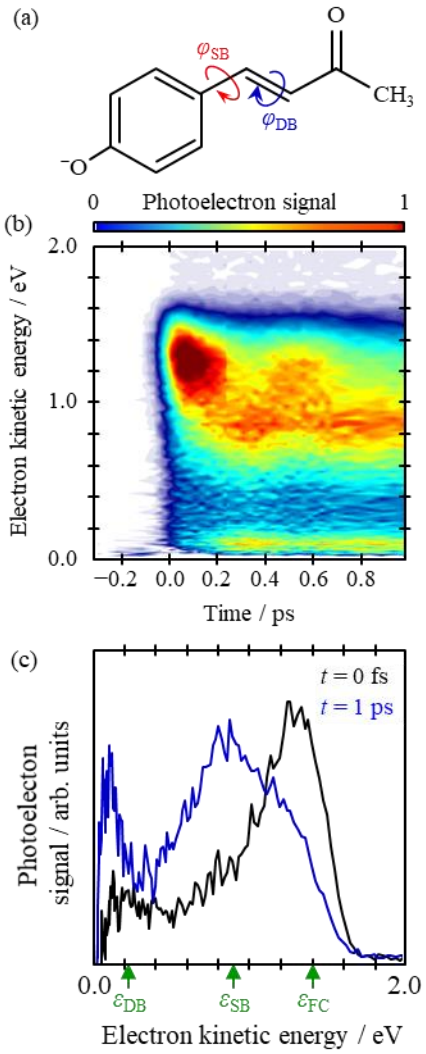

Figure 5: Time-resolved photoelectron spectroscopy of *p*CK$^-$. (a) Structure of *p*CK$^-$ and the bonds about which rotation can take place in the excited state isomerisation process. (b) Back-ground subtracted, time-resolved photoelectron spectra over the first picosecond following excitation at 2.79 eV and probing at 1.55 eV. (c) Individual photoelectron spectra at t = 0 (black) and 1 ps (blue), with green upward arrows indicating the expected maximum kinetic energy associated with detachment from the Franck-Condon geometry, ε_{FC}, the minimum following rotation about the single bond, ε_{SB}, and about the double bond, ε_{DB}. Adapted with permission from ref. 1. Copyright 2020 the authors. Published by Nature Communications under a Creative Commons Attribution 4.0 International License http://creativecommons.org/licenses/by/4.0/.

To determine which isomerisation coordinate (φ_{SB} or φ_{DB}) is probed in the experiment, Figure 6 shows the potential energy curve along these two bond rotation coordinates. These were obtained by a linear interpolation in internal coordinates (LIIC) and recalculation of the electronic energies of the S_1 and D_0 states at all points along the LIICs using multi-state XMCQDPT2, with complete details given elsewhere.[1] Spectroscopically, the photoelectron spectra are determined by the difference in energy between the S_1 and D_0 states, which evolves differently along the coordinates φ_{SB} and φ_{DB}. Specifically, at the Franck-Condon geometry, FC, we expect that probing the S_1 state with 1.55 eV will lead to photoelectron signal with eKE extending to 1.40 eV. This is in agreement with the feature seen at $t = 0$ peaking at eKE ~ 1.3 eV (Figure 5(c)). For the S_1 state evolution about the φ_{SB} coordinate, leading a twisted intermediate (SB), we anticipate that the photoelectron signal would extend to eKE = 0.87 eV, which is again in excellent agreement with the feature peaking at eKE ~ 0.8 eV in Figure 5(c). In contrast, for S_1 state evolution about the φ_{DB} coordinate, forming a twisted intermediate (DB), the signal should extend to eKE = 0.21 eV. While there is an excited state signal observed at eKE < 0.2 eV, this arises as the probe from SB becomes resonant with the S_2 state of *p*CK^-, rather than from detachment of DB, as shown by excited state calculations.[1]

Based on the above, we conclude that the photoexcited S_1 state of *p*CK^- initially isomerizes about φ_{SB}. This agrees with our[1] and others'[39,40] calculations that find a barrier along the φ_{DB} coordinate. Our experiment shows that the nuclear wavepacket along this coordinate partially returns to the planar geometry once before dephasing.

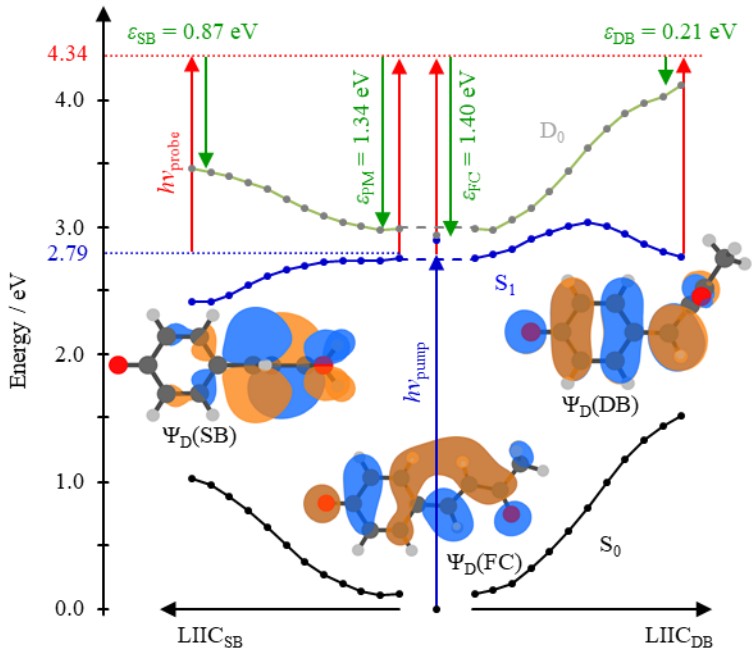

Figure 6: Potential energy curves for the S_0 and S_1 states of *p*CK$^-$ and D_0 state of the neutral as a function of isomerisation about the single bond (SB, left) and double bond (DB, right) using linear interpolation of internal coordinates. Also shown are the Dyson orbitals at the key geometries: the minimum along SB rotation, Ψ_D(SB), the Franck-Condon geometry, Ψ_D(FC), and the minimum along DB rotation, Ψ_D(DB). Vertical upward arrows indicate photo-excitation/detachment using the pump/probe pulse; downward arrows indicate the energy of the emitted electrons, with the maximal electron kinetic energies, ε, along the key geometries indicated. Adapted with permission from ref. 1. Copyright 2020 the authors. Published by Nature Communications under a Creative Commons Attribution 4.0 International License http://creativecommons.org/licenses/by/4.0/.

While the above arguments are solely based on energetic arguments, our measurements also provide information about the *electronic structure* along the isomerization pathways. In analogy to the above case of *p*EPh$^-$, rotation of the para-substituted fragment out of the plane of the ring may be expected to result in changes in the PADs.[3] Figure 7(a) shows the evolution of β_2 as a function of both eKE and t (which relates directly to spectral changes in Figure 5(b)). In Figure 7(b) and (c), β_2(eKE) is plotted at t = 0 and 1 ps, with the regions with high photoelectron signal shown as solid lines. We compare these to the predicted β_2 from the relevant Dyson orbitals, which are shown in Figure 6.

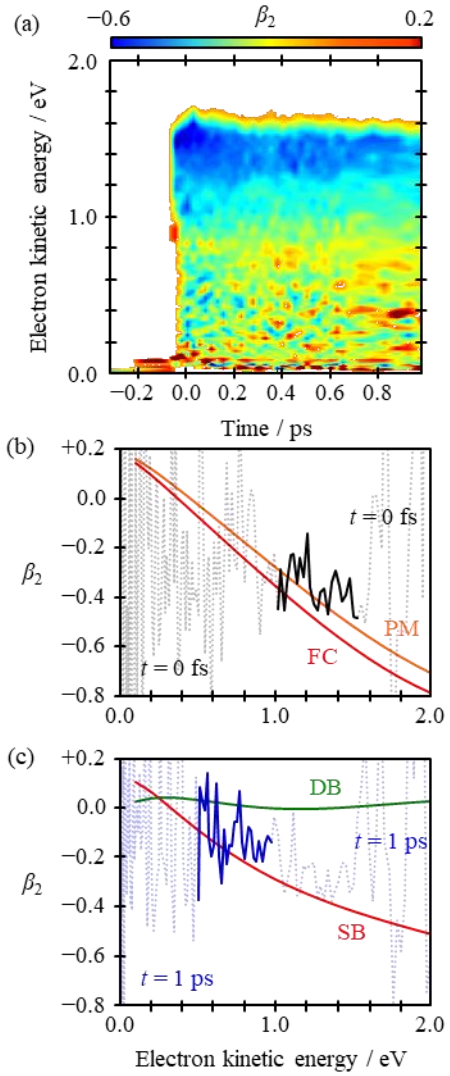

Figure 7: Time-resolved β_2 spectra. (a) A false colour plot of β_2 as a function of kinetic energy and time, which is directly comparable to the photoelectron signal in Figure 5(b). Slices of β_2 spectra taken at (b) t = 0 ps (black solid line) and (c) t = 1 ps (blue solid line). Also shown on these is the predicted β_2 spectrum from the Dyson orbitals for the key geometries in Figure 6. For t = 0 ps (b), this is comparable to the Franck-Condon geometry; For t = 1 ps (1), this is comparable to either SB rotation or DB rotation, with SB matching the data significantly better. Adapted with permission from ref. 1. Copyright 2020 the authors. Published by Nature Communications under a Creative Commons Attribution 4.0 International License http://creativecommons.org/licenses/by/4.0/.

At t = 0, we expect that the detachment will be from the S_1 state in the FC geometry and so we use this Dyson orbital, Ψ_D(FC), to calculate the β_2(eKE), as shown in Figure 7(b). The overall agreement is very good and can be made even more convincing when we account for

the initial motion on S_1 that takes the FC geometry to a planar minimum on S_1 (PM), prior to isomerization.[41] As before, we consider both φ_{SB} and φ_{DB} coordinates leading to the SB and DB intermediates. The Ψ_D of these differs and, therefore, we might anticipate that their PADs will also differ. In Figure 7(c), we compare β_2 computed from both Dyson orbitals with the experimental β_2 at t = 1 ps. The β_2 for SB is in much better agreement than that for DB, which is consistent with the conclusions from the photoelectron spectra. Hence, while the photoelectron spectra capture the *nuclear* evolution on the S_1 state, the PADs, clearly capture the *electronic* evolution. Taken holistically, we have therefore monitored the evolution of electronic character along a reaction coordinate, which is of course the basis of the Born-Oppenheimer approximation and the underpinning concept of a potential energy surface.

The predicted β_2 in Figure 7 assumed a random spatial distribution of lab-frame molecules. In principle, photoexcitation to the S_1 state could result in a pre-aligned distribution because of a defined transition dipole moment vector. Such alignment would be observable through higher order anisotropy parameters (i.e. β_4 in the present case), but these were found to be near zero indicating that no substantial pre-alignment was present in these experiments, justifying the use of the one-photon β_2 parameter.

We now briefly consider how our observations tie into the simple Hückel picture presented previously. We suggested that the S_1 state of *p*CK$^-$ could be viewed as a linear combination of π_{Ph}* and π_R*, where R = methyl vinyl ketone (or acrolein). The Hückel energy of π_R* is $\alpha - 0.38\,\beta$ (compared to $\alpha - \beta$ for π_{Ph}*) such that we expect that the S_1 state *p*CK$^-$ will be predominantly of π_R* character. As the para-bond is not directly involved in these considerations, it should come as no great surprise that there is little or no barrier to rotation about φ_{SB}. Then, once rotation sets in, the π_{Ph}* and π_R* MOs become decoupled and the S_1 electronic structure evolves to be almost exclusively of π_R* character in the SB geometry. Indeed, β_2 predicted for the π_R* fragment is in excellent agreement with that for

the SB structure. Hence, the adiabatic evolution effectively involves a charge-transfer from a delocalized MO of the FC geometry into a localized MO on the methyl vinyl ketone fragment. This evolution is primed by virtue of the π_R* character of the FC S_1 state as explained by the Hückel picture. This conclusion is pleasing as it suggests that simple Hückel theory arguments can be extended to excited states and their dynamics!

Of course, the Hückel approximations are drastic and have their limitations. One obvious limitation is non-adiabaticity, which is ultimately how the S_1 state decays to the ground electronic state of *p*CK$^-$. However, other non-adiabatic processes can take place, as we have observed in an experiment on the related chromophore in which the ketone is replaced by an ester, *p*CEs$^-$.[4] In this case, excitation to the analogous S_1 state revealed a bifurcation of the wavepacket, with some population remaining on S_1 and isomerising (as seen in *p*CK$^-$) and with another fraction non-adiabatically converting to a non-valence dipole-bound state. While the time-resolved measurements capture these dynamics fully, evidence for the interplay of non-valence states in the excited state dynamics of anions can also be seen in the single-photon photoelectron spectra of many anions.[42–44] Indeed, we have now seen the internal conversion from valence states to non-valences states (and vice versa) in a range of molecular and cluster anionic system,[45–49] where the excited state is close in energy to the detachment threshold. Why we only see the dipole-bound sate in *p*CEs$^-$ and not in *p*CK$^-$ remains unknown. The interest in anion non-valence states is growing as they are also implicated in electron capture processes and may be important even in condensed phases.[50]

Conclusions and Outlook

The ability to probe both electronic and nuclear dynamics simultaneously has been one of the key goals of chemical dynamics. Here, we have done this on a relatively large bio-molecule using a combination of established methods based around time-resolved

photoelectron imaging as a detection method. The experimental method has much scope moving forward. Specifically, progressing to larger systems is straightforward using electrospray ionisation. While this will inevitably come with enhanced complexity of the results, gas-phase spectroscopy offers tools to attain exquisite control of the initial samples. For example, the temperature can be tuned from a few 10s K to 100s K using cryogenic ion traps,[51] isomers can be preselected using ion mobility methods,[52] specific modes can be pre-excited using light fields, surroundings can be introduced in a systematic and incremental manner, and spectral/time resolution can be improved (at the expense of time/spectral resolution).[53] On the theoretical front, the computation of the PADs remains difficult. At present, there is no consideration of the spread of configurations of the nuclei, though we have recently shown that the effects of internal motion due to temperature or dynamical effects can influence the computed PADs significantly.[28] Finally, it is worth noting that there is still no robust way to compute the PADs for electron emission from resonances. Nevertheless, it is notable how well the electronic and nuclear dynamics can be tracked and correlated with computational results, offering much hope that these methods can begin to also offer new insights into more complex systems and non-adiabatic dynamics as well as the predominantly adiabatic dynamics discussed here.

We finish by marvelling at the extent to which the underlying photodynamics of a bio-chromophores can be decomposed and understood using intuitive chemical models based on Hückel theory, which offers simple tools to be exploited by general chemists to develop the photoactive protein toolbox.

Acknowledgements

We are grateful to the co-workers whose contributions along the various steps of the work presented in this Account were invaluable. Specifically, we are grateful to James Bull,

Charlie Dean and Basile Curchod. We also thank Basile Curchod for constructive comments on the manuscript. This work has been funded in parts by the EPSRC, European Research Council and Durham University.

Biographical information

Cate S. Anstöter

Cate (born in Germany, 28 October 1990) was awarded an MChem (2014) from the University of Sheffield, an MPhil (2015) from the University of Manchester and a PhD (2019) from Durham University. Following a two-year post-doc at Temple University, she is moving to the University of York to undertake a post-doc in 2022. Cate's research interests includes the photochemistry of anions and resonances from both theoretical and experimental perspectives.

Jan R. R. Verlet

Jan (born in Belgium, 6 June 1977) was awarded an MSci (1999) and PhD (2003) from King's College London. After a three-year post-doc at UC Berkeley, he moved to Durham University where he is now Professor. His research interests include electron and photon driven chemistry in the gas-phase and on aqueous surfaces.

References

(1) Anstöter, C. S.; Curchod, B. F. E.; Verlet, J. R. R. Geometric and Electronic Structure Probed along the Isomerisation Coordinate of a Photoactive Yellow Protein Chromophore. *Nat. Commun.* **2020**, *11* (1), 2827. https://doi.org/10.1038/s41467-020-16667-x.

(2) Anstöter, C. S.; Dean, C. R.; Verlet, J. R. R. Chromophores of Chromophores: A Bottom-up Hückel Picture of the Excited States of Photoactive Proteins. *Phys. Chem. Chem. Phys.* **2017**, *19* (44), 29772–29779. https://doi.org/10.1039/C7CP05766K.

(3) Anstöter, C. S.; Dean, C. R.; Verlet, J. R. R. Sensitivity of Photoelectron Angular Distributions to Molecular Conformations of Anions. *J. Phys. Chem. Lett.* **2017**, *8* (10), 2268–2273. https://doi.org/10.1021/acs.jpclett.7b00726.

(4) Bull, J. N.; Anstöter, C. S.; Verlet, J. R. R. Ultrafast Valence to Non-Valence Excited State Dynamics in a Common Anionic Chromophore. *Nat. Commun.* **2019**, *10* (1), 1–9. https://doi.org/10.1038/s41467-019-13819-6.

(5) van der Horst, M. A.; Hellingwerf, K. J. Photoreceptor Proteins, "Star Actors of Modern Times": A Review of the Functional Dynamics in the Structure of Representative Members of Six Different Photoreceptor Families. *Acc. Chem. Res.* **2004**, *37* (1), 13–20. https://doi.org/10.1021/ar020219d.

(6) Dugave, C.; Demange, L. Cis−Trans Isomerization of Organic Molecules and Biomolecules: Implications and Applications. *Chem. Rev.* **2003**, *103* (7), 2475–2532. https://doi.org/10.1021/cr0104375.

(7) Schoenlein, R. W.; Peteanu, L. A.; Mathies, R. A.; Shank, C. V. The First Step in Vision: Femtosecond Isomerization of Rhodopsin. *Science* **1991**, *254* (5030), 412–415. https://doi.org/10.1126/science.1925597.

(8) *Photophysics of Ionic Biochromophores*; Nielsen, S. B., Wyer, J. A., Eds.; Physical Chemistry in Action; Springer-Verlag: Berlin Heidelberg, 2013. https://doi.org/10.1007/978-3-642-40190-9.

(9) Geßner, O.; Lee, A. M. D.; Shaffer, J. P.; Reisler, H.; Levchenko, S. V.; Krylov, A. I.; Underwood, J. G.; Shi, H.; East, A. L. L.; Wardlaw, D. M.; Chrysostom, E. t H.; Hayden, C.

C.; Stolow, A. Femtosecond Multidimensional Imaging of a Molecular Dissociation. *Science* **2006**, *311* (5758), 219–222. https://doi.org/10.1126/science.1120779.

(10) Wörner, H. J.; Bertrand, J. B.; Kartashov, D. V.; Corkum, P. B.; Villeneuve, D. M. Following a Chemical Reaction Using High-Harmonic Interferometry. *Nature* **2010**, *466* (7306), 604–607. https://doi.org/10.1038/nature09185.

(11) Hockett, P.; Bisgaard, C. Z.; Clarkin, O. J.; Stolow, A. Time-Resolved Imaging of Purely Valence-Electron Dynamics during a Chemical Reaction. *Nat. Phys.* **2011**, *7* (8), 612–615. https://doi.org/10.1038/nphys1980.

(12) Peng, P.; Marceau, C.; Villeneuve, D. M. Attosecond Imaging of Molecules Using High Harmonic Spectroscopy. *Nat. Rev. Phys.* **2019**, *1* (2), 144–155. https://doi.org/10.1038/s42254-018-0015-1.

(13) Yang, J.; Zhu, X.; Nunes, J. P. F.; Yu, J. K.; Parrish, R. M.; Wolf, T. J. A.; Centurion, M.; Gühr, M.; Li, R.; Liu, Y.; Moore, B.; Niebuhr, M.; Park, S.; Shen, X.; Weathersby, S.; Weinacht, T.; Martinez, T. J.; Wang, X. Simultaneous Observation of Nuclear and Electronic Dynamics by Ultrafast Electron Diffraction. *Science* **2020**, *368* (6493), 885–889. https://doi.org/10.1126/science.abb2235.

(14) Hellingwerf, K. J.; Hendriks, J.; Gensch, T. Photoactive Yellow Protein, A New Type of Photoreceptor Protein: Will This "Yellow Lab" Bring Us Where We Want to Go? *J. Phys. Chem. A* **2003**, *107* (8), 1082–1094. https://doi.org/10.1021/jp027005y.

(15) Kort, R.; Vonk, H.; Xu, X.; Hoff, W. D.; Crielaard, W.; Hellingwerf, K. J. Evidence for Trans-Cis Isomerization of the p-Coumaric Acid Chromophore as the Photochemical Basis of the Photocycle of Photoactive Yellow Protein. *FEBS Lett.* **1996**, *382* (1–2), 73–78. https://doi.org/10.1016/0014-5793(96)00149-4.

(16) Lee, I.-R.; Lee, W.; Zewail, A. H. Primary Steps of the Photoactive Yellow Protein: Isolated Chromophore Dynamics and Protein Directed Function. *Proc. Natl. Acad. Sci.* **2006**, *103* (2), 258–262. https://doi.org/10.1073/pnas.0510015103.

(17) Kuramochi, H.; Takeuchi, S.; Kamikubo, H.; Kataoka, M.; Tahara, T. Fifth-Order Time-Domain Raman Spectroscopy of Photoactive Yellow Protein for Visualizing Vibrational Coupling in Its Excited State. *Sci. Adv.* **2019**, *5* (6), eaau4490. https://doi.org/10.1126/sciadv.aau4490.

(18) Tenboer, J.; Basu, S.; Zatsepin, N.; Pande, K.; Milathianaki, D.; Frank, M.; Hunter, M.; Boutet, S.; Williams, G. J.; Koglin, J. E.; Oberthuer, D.; Heymann, M.; Kupitz, C.; Conrad, C.; Coe, J.; Roy-Chowdhury, S.; Weierstall, U.; James, D.; Wang, D.; Grant, T.; Barty, A.; Yefanov, O.; Scales, J.; Gati, C.; Seuring, C.; Srajer, V.; Henning, R.; Schwander, P.; Fromme, R.; Ourmazd, A.; Moffat, K.; Thor, J. J. V.; Spence, J. C. H.; Fromme, P.; Chapman, H. N.; Schmidt, M. Time-Resolved Serial Crystallography Captures High-Resolution Intermediates of Photoactive Yellow Protein. *Science* **2014**, *346* (6214), 1242–1246. https://doi.org/10.1126/science.1259357.

(19) Eppink, A. T. J. B.; Parker, D. H. Velocity Map Imaging of Ions and Electrons Using Electrostatic Lenses: Application in Photoelectron and Photofragment Ion Imaging of Molecular Oxygen. *Rev. Sci. Instrum.* **1997**, *68* (9), 3477–3484. https://doi.org/10.1063/1.1148310.

(20) Reid, K. L. Photoelectron Angular Distributions. *Annu. Rev. Phys. Chem.* **2003**, *54* (1), 397–424. https://doi.org/10.1146/annurev.physchem.54.011002.103814.

(21) Cooper, J.; Zare, R. N. Angular Distribution of Photoelectrons. *J. Chem. Phys.* **1968**, *48* (2), 942–943. https://doi.org/10.1063/1.1668742.

(22) Corderman, R. R.; Lineberger, W. C. Negative Ion Spectroscopy. *Annu. Rev. Phys. Chem.* **1979**, *30* (1), 347–378. https://doi.org/10.1146/annurev.pc.30.100179.002023.

(23) Zimmerman, A. H.; Brauman, J. I. Resonances in Electron Photodetachment Cross Sections. *J. Chem. Phys.* **1977**, *66* (12), 5823–5825. https://doi.org/10.1063/1.433860.

(24) Lecointre, J.; Roberts, G. M.; Horke, D. A.; Verlet, J. R. R. Ultrafast Relaxation Dynamics Observed Through Time-Resolved Photoelectron Angular Distributions. *J. Phys. Chem. A* **2010**, *114* (42), 11216–11224. https://doi.org/10.1021/jp1028855.

(25) Stanley, L. H.; Anstöter, C. S.; Verlet, J. R. R. Resonances of the Anthracenyl Anion Probed by Frequency-Resolved Photoelectron Imaging of Collision-Induced Dissociated Anthracene Carboxylic Acid. *Chem. Sci.* **2017**, *8* (4), 3054–3061. https://doi.org/10.1039/C6SC05405F.

(26) Oana, C. M.; Krylov, A. I. Cross Sections and Photoelectron Angular Distributions in Photodetachment from Negative Ions Using Equation-of-Motion Coupled-Cluster Dyson Orbitals. *J. Chem. Phys.* **2009**, *131* (12), 124114. https://doi.org/10.1063/1.3231143.

(27) Gozem, S.; Krylov, A. I. The EzSpectra Suite: An Easy-to-Use Toolkit for Spectroscopy Modeling. *WIREs Comput. Mol. Sci. n/a* (n/a), e1546. https://doi.org/10.1002/wcms.1546.

(28) Anstöter, C. S.; Verlet, J. R. R. Modeling the Photoelectron Angular Distributions of Molecular Anions: Roles of the Basis Set, Orbital Choice, and Geometry. *J. Phys. Chem. A* **2021**, *125* (22), 4888–4895. https://doi.org/10.1021/acs.jpca.1c03379.

(29) Sanov, A. Laboratory-Frame Photoelectron Angular Distributions in Anion Photodetachment: Insight into Electronic Structure and Intermolecular Interactions. *Annu. Rev. Phys. Chem.* **2014**, *65* (1), 341–363. https://doi.org/10.1146/annurev-physchem-040513-103656.

(30) Bravaya, K. B.; Grigorenko, B. L.; Nemukhin, A. V.; Krylov, A. I. Quantum Chemistry Behind Bioimaging: Insights from Ab Initio Studies of Fluorescent Proteins and

Their Chromophores. *Acc. Chem. Res.* **2012**, *45* (2), 265–275. https://doi.org/10.1021/ar2001556.

(31) Bochenkova, A. V.; Klærke, B.; Rahbek, D. B.; Rajput, J.; Toker, Y.; Andersen, L. H. UV Excited-State Photoresponse of Biochromophore Negative Ions. *Angew. Chem. Int. Ed.* **2014**, *53* (37), 9797–9801. https://doi.org/10.1002/anie.201404609.

(32) Anstöter, C. S.; Bull, J. N.; Verlet, J. R. R. Ultrafast Dynamics of Temporary Anions Probed through the Prism of Photodetachment. *Int. Rev. Phys. Chem.* **2016**, *35* (4), 509–538. https://doi.org/10.1080/0144235X.2016.1203522.

(33) West, C. W.; Bull, J. N.; Antonkov, E.; Verlet, J. R. R. Anion Resonances of Para-Benzoquinone Probed by Frequency-Resolved Photoelectron Imaging. *J. Phys. Chem. A* **2014**, *118* (48), 11346–11354. https://doi.org/10.1021/jp509102p.

(34) Lietard, A.; Verlet, J. R. R.; Slimak, S.; Jordan, K. D. Temporary Anion Resonances of Pyrene: A 2D Photoelectron Imaging and Computational Study. *J. Phys. Chem. A* **2021**, *125* (32), 7004–7013. https://doi.org/10.1021/acs.jpca.1c05586.

(35) West, C. W.; Bull, J. N.; Hudson, A. S.; Cobb, S. L.; Verlet, J. R. R. Excited State Dynamics of the Isolated Green Fluorescent Protein Chromophore Anion Following UV Excitation. *J. Phys. Chem. B* **2015**, *119* (10), 3982–3987. https://doi.org/10.1021/acs.jpcb.5b01432.

(36) Horke, D. A.; Verlet, J. R. R. Photoelectron Spectroscopy of the Model GFP Chromophore Anion. *Phys. Chem. Chem. Phys.* **2012**, *14* (24), 8511–8515. https://doi.org/10.1039/c2cp40880e.

(37) Zagorec-Marks, W.; Foreman, M. M.; Verlet, J. R. R.; Weber, J. M. Cryogenic Ion Spectroscopy of the Green Fluorescent Protein Chromophore in Vacuo. *J. Phys. Chem. Lett.* **2019**, *10* (24), 7817–7822. https://doi.org/10.1021/acs.jpclett.9b02916.

(38) Bochenkova, A. V.; Andersen, L. H. Ultrafast Dual Photoresponse of Isolated Biological Chromophores: Link to the Photoinduced Mode-Specific Non-Adiabatic Dynamics in Proteins. *Faraday Discuss.* **2013**, *163* (0), 297–319. https://doi.org/10.1039/C3FD20150C.

(39) Groenhof, G.; Bouxin-Cademartory, M.; Hess, B.; de Visser, S. P.; Berendsen, H. J. C.; Olivucci, M.; Mark, A. E.; Robb, M. A. Photoactivation of the Photoactive Yellow Protein: Why Photon Absorption Triggers a Trans-to-Cis Isomerization of the Chromophore in the Protein. *J. Am. Chem. Soc.* **2004**, *126* (13), 4228–4233. https://doi.org/10.1021/ja039557f.

(40) Boggio-Pasqua, M.; Groenhof, G. On the Use of Reduced Active Space in CASSCF Calculations. *Comput. Theor. Chem.* **2014**, *1040–1041*, 6–13. https://doi.org/10.1016/j.comptc.2014.03.017.

(41) Anstöter, C. S.; Curchod, B. F. E.; Verlet, J. R. R. Photo-Isomerization of the Isolated Photoactive Yellow Protein Chromophore: What Comes before the Primary Step? *Phys. Chem. Chem. Phys.* **2022**, *24* (3), 1305–1309. https://doi.org/10.1039/D1CP05259D.

(42) Anstöter, C. S.; Mensa-Bonsu, G.; Nag, P.; Ranković, M.; Kumar T. P., R.; Boichenko, A. N.; Bochenkova, A. V.; Fedor, J.; Verlet, J. R. R. Mode-Specific Vibrational Autodetachment Following Excitation of Electronic Resonances by Electrons and Photons. *Phys. Rev. Lett.* **2020**, *124* (20), 203401. https://doi.org/10.1103/PhysRevLett.124.203401.

(43) Anstöter, C. S.; Verlet, J. R. R. Gas-Phase Synthesis and Characterization of the Methyl-2,2-Dicyanoacetate Anion Using Photoelectron Imaging and Dipole-Bound State Autodetachment. *J. Phys. Chem. Lett.* **2020**, *11* (15), 6456–6462. https://doi.org/10.1021/acs.jpclett.0c02036.

(44) Bull, J. N.; Anstöter, C. S.; Verlet, J. R. R. Fingerprinting the Excited State Dynamics in Methyl Ester and Methyl Ether Anions of Deprotonated Para-Coumaric Acid. *J. Phys. Chem. A* **2020**. https://doi.org/10.1021/acs.jpca.9b11993.

(45) Bull, J. N.; West, C. W.; Verlet, J. R. R. Ultrafast Dynamics of Formation and Autodetachment of a Dipole-Bound State in an Open-Shell π-Stacked Dimer Anion. *Chem. Sci.* **2016**, *7* (8), 5352–5361. https://doi.org/10.1039/C6SC01062H.

(46) Bull, J. N.; Verlet, J. R. R. Observation and Ultrafast Dynamics of a Nonvalence Correlation-Bound State of an Anion. *Sci. Adv.* **2017**, *3* (5), e1603106. https://doi.org/10.1126/sciadv.1603106.

(47) Rogers, J. P.; Anstöter, C. S.; Verlet, J. R. R. Ultrafast Dynamics of Low-Energy Electron Attachment via a Non-Valence Correlation-Bound State. *Nat. Chem.* **2018**, *10* (3), 341–346. https://doi.org/10.1038/nchem.2912.

(48) Rogers, J. P.; Anstöter, C. S.; Verlet, J. R. R. Evidence of Electron Capture of an Outgoing Photoelectron Wave by a Nonvalence State in (C6F6)n–. *J. Phys. Chem. Lett.* **2018**, *9* (10), 2504–2509. https://doi.org/10.1021/acs.jpclett.8b00739.

(49) Verlet, J. R. R.; Anstöter, C. S.; Bull, J. N.; Rogers, J. P. Role of Nonvalence States in the Ultrafast Dynamics of Isolated Anions. *J. Phys. Chem. A* **2020**, *124* (18), 3507–3519. https://doi.org/10.1021/acs.jpca.0c01260.

(50) Castellani, M. E.; Anstöter, C. S.; Verlet, J. R. R. On the Stability of a Dipole-Bound State in the Presence of a Molecule. *Phys. Chem. Chem. Phys.* **2019**, *21* (44), 24286–24290. https://doi.org/10.1039/C9CP04942H.

(51) Wang, X.-B.; Wang, L.-S. Development of a Low-Temperature Photoelectron Spectroscopy Instrument Using an Electrospray Ion Source and a Cryogenically Controlled Ion Trap. *Rev. Sci. Instrum.* **2008**, *79* (7), 073108. https://doi.org/10.1063/1.2957610.

(52) Warnke, S.; Faleh, A. B.; Pellegrinelli, R. P.; Yalovenko, N.; Rizzo, T. R. Combining Ultra-High Resolution Ion Mobility Spectrometry with Cryogenic IR Spectroscopy for the Study of Biomolecular Ions. *Faraday Discuss.* **2019**, *217* (0), 114–125. https://doi.org/10.1039/C8FD00180D.

(53) Kang, D. H.; An, S.; Kim, S. K. Real-Time Autodetachment Dynamics of Vibrational Feshbach Resonances in a Dipole-Bound State. *Phys. Rev. Lett.* **2020**, *125* (9), 093001. https://doi.org/10.1103/PhysRevLett.125.093001.